Journal of Environmental Chemical Engineering 13 (2025) 116998

Contents lists available at ScienceDirect

Journal of Environmental Chemical Engineering

journal homepage: www.elsevier.com/locate/jece

Photoreforming of PET and PLA microplastics for sustainable hydrogen production using TiO_2 and g-C_3N_4 photocatalysts

Petr Praus [a,b,*], Lenka Řeháčková [c], Miroslava Filip-Edelmanová [a], Anna Gavlová [a,d], Martin Koštejn [e], Radim Škuta [c], Jan Bednárek [a], Petr Bednář [d], Kamila Kočí [a,f]

[a] Institute of Environmental Technology, CEET, VSB-Technical University of Ostrava , 17. listopadu 15, Ostrava, Poruba 708 00, Czech Republic
[b] Department of Chemistry, Faculty of Science, University of Ostrava, 30. dubna 22, Ostrava 701 03, Czech Republic
[c] Department of Chemistry and Physico-Chemical Processes, Faculty of Materials Science and Technology, VSB-Technical University of Ostrava, Poruba, Ostrava 708 00, Czech Republic
[d] Department of Analytical Chemistry, Faculty of Science, Palacky University, 17. listopadu 12, Olomouc 779 00, Czech Republic
[e] Institute of Chemical Process Fundamentals, Czech Academy of Science, Rozvojová 1, Prague 165 02, Czech Republic
[f] Department of Physics and Materials Engineering, Faculty of Technology, Tomas Bata University in Zlín, Vavrečkova 275, Czech Republic

ARTICLE INFO

Keywords:
Microplastics
PET
PLA
Photoreforming
Hydrogen
G-C_3N_4 instability

ABSTRACT

Photoreforming of polyethylene terephthalate (PET) and polylactic acid (PLA) microplastics has been investigated as a sustainable approach for hydrogen evolution. Thermodynamic analysis confirmed the feasibility of hydrogen evolution during the degradation of PET and PLA under UV irradiation (254 nm). Photolysis experiments in water demonstrated that hydrogen, methane, and carbon monoxide were the primary gaseous products. PLA yields higher amounts of hydrogen than PET. The presence of NaOH significantly reduced hydrogen evolution, likely because of the scavenging of hydrogen radicals with hydroxide ions and neutralisation of carboxylic groups. Photocatalytic experiments in water using TiO_2 and graphitic carbon nitride (g-C_3N_4) further increased the hydrogen yields of PET and PLA, with a more pronounced effect on PLA. However, in NaOH suspensions, hydrogen evolution increased only for PLA in the presence of TiO_2, while g-C_3N_4 had no effect. This was attributed to the instability of g-C_3N_4 under alkaline conditions, as confirmed by the structural analysis.

1. Introduction

Plastic materials are durable, cheap, and light materials that have been used for many human activities. As plastic materials are versatile, their production was 360 million tons in 2018, and plastic production in 2025 was assumed to reach 500 million tons [1]. In a review article by Napper and Thomson [2], all aspects of plastic waste were well summarised.

Plastic microparticles, often called microplastics, are a matter of growing concern from the environmental, health, and regulatory perspectives. The presence of microplastics in seawater was first reported by Thomson et al. in 2004 [3]. Microplastics are a part of products such as cosmetics (microbeads in exfoliating scrubs) and industrial abrasives, and are even used in air blasting technology. These microplastics (primary microplastics) enter the environment directly from various sources. Other microplastics (secondary microplastics) are larger plastics, such as plastic bottles, bags, and fishing nets. Various weathering processes, including photodegradation, mechanical abrasion, and other environmental factors, break plastics into smaller fragments. They exist in various forms, such as spheres, fragments, and fibres. Owing to their small size, they can easily enter ecosystems and be ingested by a wide range of organisms, including aquatic organisms and humans. It should be noted that there is no clear size limit for microplastics. Some authors consider microplastics to be plastic particles with sizes between 1 μm and 5 mm.

Environmental microplastics in the environment have attracted the attention of many scientists worldwide. The number of reviews and research articles on microplastics has been increasing annually (see Fig. 1S in the Supplementary Materials). Their occurrence in water [4,5], soil [5,6], the human body [7], fish [8], plants [9], the atmosphere [10], and food [11] has been reported. For example, refer to other review articles on the topic of microplastics [12–16].

* Corresponding author at: Institute of Environmental Technology, CEET, VSB-Technical University of Ostrava, 17. listopadu 15, Poruba, Ostrava 708 00, Czech Republic.
E-mail address: petr.praus@vsb.cz (P. Praus).

https://doi.org/10.1016/j.jece.2025.116998
Received 18 February 2025; Received in revised form 13 April 2025; Accepted 7 May 2025
Available online 8 May 2025
2213-3437/© 2025 The Authors. Published by Elsevier Ltd. This is an open access article under the CC BY license (http://creativecommons.org/licenses/by/4.0/).

Various technologies have been established for the retention of microplastics, such as coagulation, membrane filtration, adsorption, and degradation, based on oxidation processes [17,18], catalysis [19,20], and biodegradation processes [21]. For example, microplastics in wastewater can be effectively removed by conventional treatment processes with an efficiency of up to 99 % (more than 65 % remains in sewage sludge) without their useful degradation [14,22,23]. Therefore, technologies for both degradation and recycling must be developed. Recycling technologies enable the reduction of the amount of microplastics and, in addition, transform them into useful products also known as "trash to treasure." They are based on i) chemical recycling of oil/hydrocarbon components or high-purity chemicals [24,25], ii) energy recycling by heating (pyrolysis), and iii) light absorption (photoreforming) [22,26–31].

Photoreforming of microplastics is emerging as a dual-benefit technology, offering both environmental remediation and the generation of valuable products such as hydrogen and organic chemicals. This process uses photocatalysis under solar or artificial light to break down microplastics in aqueous media and convert them into simpler molecules. Photoreforming of PET and PLA waste-forming hydrogen has been reported using MoS_2-Tipped CdS nanorods [32], defect-rich $NiPS_3$ nanosheets [33], heterojunction Ni_3S_4/ZnCdS photocatalysts [34], high-pressure columbite phase of titanium dioxide [35], and B-doped carbon nitride nanotubes [36]. Photoreforming of PE using g-C_3N_4/Co_3O_4 Z-scheme heterostructure [37]. Comprehensive review articles on the photoreforming of plastics have been published [38–43].

Photoreforming has recently been reviewed as an emerging process for plastic waste treatment. The scalability of photoreforming, its low energy demand, and the avoidance of toxic by-products make it a compelling solution for microplastic pollution. However, challenges, such as catalyst durability, broad-spectrum light absorption, and real-world applications under mixed plastic waste conditions remain as focal points for future research.

The aim of this study was to investigate the photoreforming of selected microplastics, such as PET and PLA, to obtain useful products in the gaseous phase, particularly hydrogen. Before the laboratory experiments were performed, the feasibility of this process was confirmed by analysing thermodynamic data. Hydrogen was then evolved *via* photolysis and photocatalysis under UV irradiation. Photocatalytic experiments were performed using TiO_2 and g-C_3N_4 photocatalysts.

2. Experimental

2.1. Chemicals

Titanium dioxide (Degussa P25) and melamine were obtained from Sigma-Aldrich (Darmstadt, Germany), NaOH was obtained from Lach-Ner (Neratovice, Czech Republic), and helium (5.0) was obtained from Messer Technogas (Ostrava, Czech Republic). Granulated PLA and PET were obtained from the TotalEnergies Corbion (Gorinchem, Netherlands) and Selenis (Portalegre, Portugal), respectively. Distilled water was used for all experiments.

2.2. Synthesis of photocatalysts

Titanium dioxide (Degussa P25) was obtained as a commercial product. Bulk g-C_3N_4 was synthesized by the direct heating of melamine at 550 °C for 4 h with a heating rate of 3 °C·min^{-1}. Melamine (5 g) was placed in a ceramic crucible with a lid in a muffle furnace. The crucible was then cooled to room temperature outside the furnace and ground into a fine powder in a laboratory mill. Bulk g-C_3N_4 was exfoliated by heating a thin layer on a ceramic plate (diameter 8 cm, 50 mL) at 500°C in a muffle furnace for 3 h at a heating rate of 10°C. min^{-1}. The ceramic plate containing the product was cooled from the furnace to room temperature.

The exfoliation was performed under the same conditions as those used for the synthesis of bulk g-C_3N4. The thermal exfoliation of g-C_3N_4 was found to be a simple procedure for the synthesis of highly efficient photocatalyst [44–46]. Some characteristics of both photocatalysts are shown in Supplementary materials

2.3. Preparation of microplastics

The polymer granulates of PET and PLA were ground in a cryogenic mill CryoMill (Retsch GmbH, Haan, Germany), and the granulometry was adjusted to 160 μm using an analytical sieve shaker AS200 (Restch, Haan, Germany) and a sieve using Preciselekt (Dolní Loučky, Czech Republic).

2.4. Characterization of microplastics

2.4.1. Elemental analysis and calorimetry

Elemental analysis (EA) of oxygen, carbon, and hydrogen in microplastics was performed using a Flash 2000 elemental analyser (Thermo Fisher Scientific, Waltham, MA, USA). The carbon and hydrogen contents were directly determined, and the oxygen content was calculated

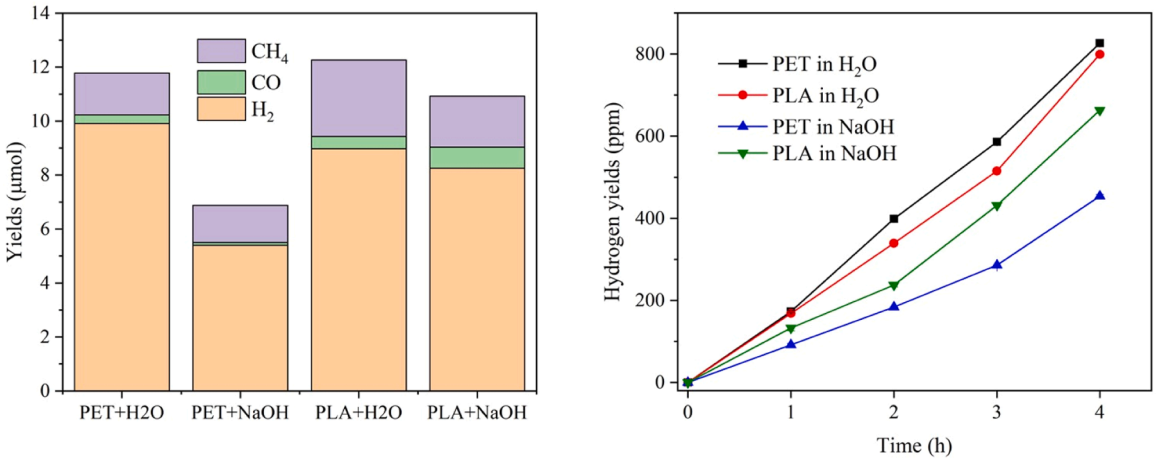

Fig. 1. Yields of the three main gaseous products of PET and PLA degradation after 4 h (left) and hydrogen yields during photolysis (right) under irradiation at 254 nm.

to be up to 100 %. The combustion heats of PET and PLA were determined using a calorimeter LECO AC600 (LECO Corporation, Michigan, USA). The plastic samples (0.25 g) were burned in an oxygen atmosphere.

2.4.2. Fourier transform infrared spectroscopy

Fourier-transform infrared (FTIR) spectra were obtained using a Thermo Scientific Nicolet iS10 FTIR Spectrometer. The measurements were carried out in the range of 500–4000 cm^{-1} with a resolution of 2 cm^{-1} using the ATR mode with a Smart iTX attachment. A small amount of the sample was placed on a diamond measuring window on an ATR attachment where the spectrum was collected. Each spectrum consisted of at least 64 scans, each lasting 1 s. Before each measurement, the background was collected to eliminate the apparatus and environmental effects. The spectra of each sample were rationed.

2.4.3. X-ray powder diffraction

X-ray powder diffraction (XRD) patterns were obtained using a Rigaku SmartLab diffractometer (Rigaku, Tokyo, Japan) equipped with a D/teX Ultra 250 detector. The X-ray irradiation source was a Cu tube (Cu Kα, $\lambda_1 = 0.154059$ nm, $\lambda_2 = 0.154441$ nm) operated at 40 kV and 30 mA. The incident and diffracted beam optics were equipped with 5° Soller slits; the incident slits were set to 1° (fixed divergence slits). Both the slits on the diffracted beam were set to a fixed value of 1 mm. The powder samples were measured in reflection mode (Bragg-Brentano geometry). The samples were rotated (30 rpm) during the measurement to eliminate the preferred orientation effects. The XRD patterns were collected in the 2θ range of 5–90° with a step size of 0.01° and a speed of 0.5 $deg.min^{-1}$.

2.4.4. X-Ray photoelectron spectroscopy

Superficial elemental analysis was performed using an X-ray photoelectron spectrometer (XPS) ESCA 3400 (Kratos Analytical Ltd, UK) with a base pressure in an analysis chamber of 5.0×10^{-7} Pa. The powdered materials were placed on conductive carbon tape. The electrons were excited using Mg Kα radiation ($h\nu = 1253.6$ eV) generated at 12 kV and 10 mA. For all the spectra, the Shirley background was subtracted. Peaks ascribed to sp^2 hybridized nitrogen (C═N-C) were set to 398.8 eV as a charge correction. The XPS spectra of boric acid and cyanoguanidine were corrected by C 1 s set to 284.8 eV as they do not contain sp^2 hybridized nitrogen.

2.4.5. Scanning electron microscopy

A scanning electron microscope (SEM) Tescan Vega (Tescan Orsay Holding, Brno, Czech Republic) with a tungsten cathode and energy-dispersive X-ray spectroscopy (EDAX, Ametex, PA, USA) were used for microscopic investigation of the powder samples. SEM micrographs were obtained using the backscattered (BSE) and secondary electron (SE) modes to determine the benefits of both techniques while reducing the impact of their drawbacks.

2.5. Photochemical experiments

The photolytic and photocatalytic experiments were conducted in a batch photoreactor with a volume of 348 mL (Fig. 2S). Photolytic tests (with no photocatalysts) were performed using reaction mixtures consisting of 100 mL of deionised water or NaOH solution (0.2 mol L^{-1}) and 0.5 g of the investigated plastic materials. The reactor was tightly sealed and the mixture was purged with helium. An UV 254 nm pen-ray lamp was employed as a source of illumination and positioned on a quartz glass window at the top of the photoreactor. The samples of the gaseous phase were taken through a septum using a syringe and analysed using a gas chromatograph (GC, Shimadzu Nexis GC-2030) equipped with a dielectric barrier discharge ionisation detector (BID). The separation was performed using an analytical column (2 m x 0.52 mm i.d., carbon molecular sieve (ShinCarbon ST) with a specific surface area of 1500 m^2

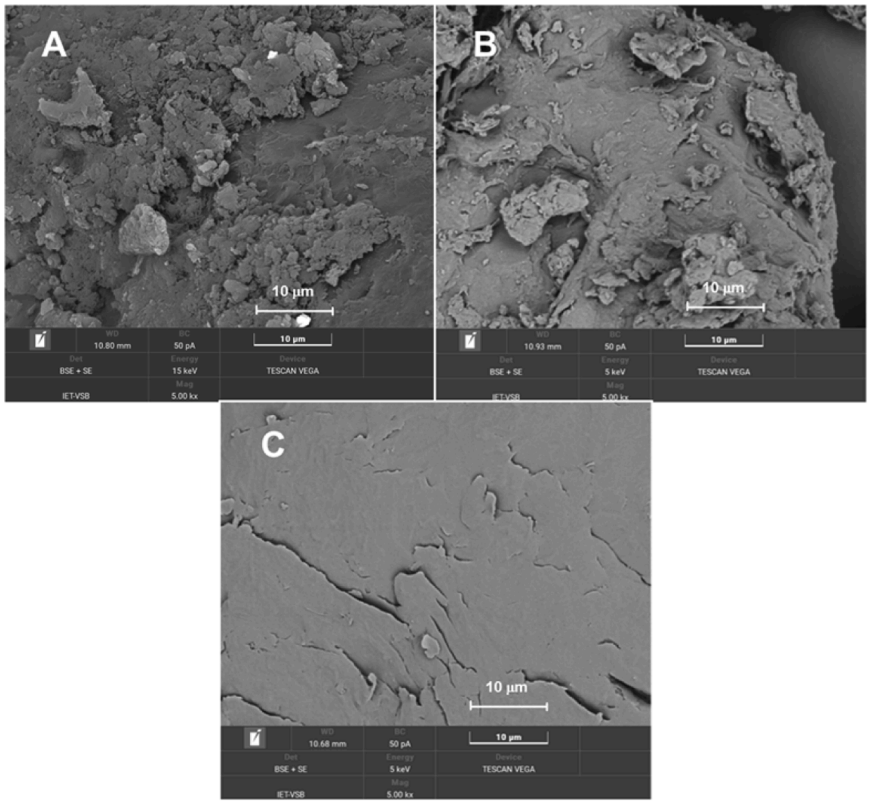

Fig. 2. SEM micrographs of PET microplastics used for photolysis. (A) Original microplastics, (B) microplastics after 24 h in water, and (C) microplastics after 24 h in NaOH.

g^{-1}) (Restek Corporation, Bellefonte, PA, USA). The reaction mixtures were exposed to irradiation for 4 h, and gaseous samples were taken at time intervals of 1, 2, 3, and 4 h for GC-BID analysis.

Photocatalytic tests with TiO_2 and g-C_3N_4 were carried out using deionised water and reaction mixtures consisting of 100 mL of a suspension (0.5 g) of the investigated plastic materials (and with the addition 0.05 g of TiO_2 to a NaOH suspension). All photochemical experiments were repeated three times to ensure reproducible results. The characterisation results of the TiO_2 and g-C_3N_4 photocatalysts are shown in the Supplementary Materials (see Tables 1S and 2S and Fig. 3S-7S).

2.6. Identification of photoreforming products

The identification and characterisation of the degradation products (DPs) of the photolysis and photocatalysis of PLA and PET were performed using liquid chromatography combined with high-resolution tandem mass spectrometry (HPLC/HRTMS). To determine the DPs, approximately 10 mL aliquots were taken after the termination of the photocatalytic and photolytic experiments. Aliquots were filtered using Chromafil GF/RC-20/25 syringe filters (pore size 0.2–1.0 μm). Blank samples were prepared using the same method used for photolysis and photocatalysis, but without adding the plastic microparticles (the deionised water/NaOH solution was irradiated in the photoreactor for 4 h with and without the photocatalyst).

HPLC/HRTMS analysis of these samples was performed with an Acquity UPLC system coupled to a high-resolution tandem mass spectrometer (Synapt G2-S; Waters, Massachusetts, USA). A Raptor Polar X analytical column (100 mm×2.1 mm i.d., 2.7 μm particles (Restek Corporation, Bellefonte, PA, USA) was used for the chromatographic separation along with a mobile phase consisting of ultrapure water (A) and acetonitrile (B), both acidified with 0.1 % of formic acid. An applied gradient method was as follows: starts with 50 % B, increasing up to 70 % B in 4.5 min, then increasing again up to 100 % B in 3 min, held there for 2.5 min, then decreasing down to 50 % B in 55 s, and held there for 1 min and 5 s. The injection volume was 5 μL, and the flow rate was 0.25 mL min^{-1}. The parameters of the mass spectrometer were as follows: spray voltage of + 2 kV, sample cone voltage of 15 V, source temperature of 300°C, desolvation temperature of 350°C, desolvation gas flow of 600 l h^{-1}, analyser in V-mode, scan range of 50–1200 (Da), scan time of 0.2 s, and interscan delay of 0.02 s. MS/MS data were obtained via fragmentation experiments in a trap-collision cell. Collision energy of 25 eV was used.

3. Results and discussion

3.1. Thermodynamic analysis

Feasibility of the photoreforming of both microplastics to obtain hydrogen was considered based on the thermodynamic analysis of the degradation of PET and PLA according to reactions

$$C_{10}H_8O_4(s) + 16\ H_2O(l) \rightarrow 10\ CO_2(g) + 20\ H_2(g) \quad (1)$$

$$C_3H_4O_2(s) + 4\ H_2O(l) \rightarrow 3\ CO_2(g) + 6\ H_2(g) \quad (2)$$

The change of the standard Gibbs energy ($\Delta_r G^0_{298}$) of these reactions was calculated according to the common equation

$$\Delta_r G^0_{298} = \Delta_r H^0_{298} - T\Delta_r S^0_{298} \quad (3)$$

Table 1
Determined combustion and calculated formation enthalpies of PET and PLA.

Plastics	$\Delta H^0_{298,comb}$ (kJ mol^{-1})	$\Delta H^0_{298,f}$ (kJ mol^{-1})
PET	−4650	−253
PLA	−1350	−314

Table 2
Calculated reaction enthalpies, entropies, and Gibbs energies.

Plastics	$\Delta_r H^0_{298}$ (kJ mol^{-1})	$\Delta_r S^0_{298}$(kJ K^{-1} mol^{-1})	$\Delta_r G^0_{298}$(kJ mol^{-1})
PET (reaction 1)	891	3.59	−181
PLA (reaction 2)	277	1.13	−61.0
PLA (reaction 2)	277	1.11	−55.1

where $\Delta_r H^0_{298}$, T, $\Delta_r S^0_{298}$ are reaction enthalpy, absolute temperature, and reaction entropy. The reaction enthalpy ($\Delta_r H^0_{298}$) was calculated based on the formation enthalpies of the substances involved in the reactions (1) and (2). The formation enthalpies $\Delta H^0_{298,f}$ of $C_{10}H_8O_4$ (PET) and $C_3H_4O_2$ (PLA) were calculated according to their combustion reactions (1S) and (2S), see Supplementary Materials. The reaction enthalpies of these combustion reactions ($\Delta_r H^0_{298}$) were substituted with the combustion enthalpies $\Delta H^0_{298,comb}$ determined by calorimetry, see Table 1. Then, the formation enthalpies ($\Delta H^0_{298,f}$) of PET and PLA were calculated from the Hess equation (Eq. 3S), see Table 2.

Similarly, reaction entropies ($\Delta_r S^0_{298}$) were calculated as the difference between the entropies of the products and reactants involved in the reactions (1) and (2) according to Eq. (4S). The standard enthalpies and entropies used in the calculations are summarised in Table 3S. The standard entropies (ΔS^0_{298}) of PET and PLA were adopted from literature [47]. As there are two ΔS^0_{298} values for PLA (Table 2) the reaction Gibbs energies were calculated for both. The enthalpies, entropies, and the Gibbs energies of the reactions (1) and (2) according to Eq. (3) are summarised in Table 2.

All the calculated values of $\Delta_r G^0_{298} < 0$ indicate that the reactions (1) and (2) are thermodynamically feasible. Therefore, photoreforming experiments were performed with both microplastics, as discussed below. Moreover, these reaction Gibbs energies are lower than that of water splitting ($2\ H_2O \rightarrow O_2 + 2\ H_2$) which is 237 kJ mol^{-1}. This indicates that the evolution of hydrogen from (micro)plastics is more feasible than that from water and deserves further investigation.

3.2. Photolysis of microplastics

Microplastics for the photoreforming experiments were obtained by milling and sieving PLA and PET granulates to obtain particles with sizes of 160 ≤ μm. Their real compositions were determined by elemental analysis and compared with the theoretical compositions calculated from their monomer formulas (see Table 3). It is evident that the experimental and theoretical data agree well.

In general, photolysis refers to the direct dissociation of chemical bonds in microplastic polymers by the absorption of UV light, leading to the formation of reactive radicals such as hydrogen radicals. The photolysis of PET and PLA microplastics was performed under UV irradiation at 254 nm in the water and NaOH suspensions. NaOH was supposed to provide more efficient hydrolysis of PET and PLA ester bonds [38]. Three main gaseous products were identified, namely hydrogen, methane, and carbon monoxide (Fig. 1). The yields of these products followed the order: $H_2 > CH_4 > CO$. These results suggest that photolysis leads to the formation of organic compounds in the liquid phase.

Fig. 1 (right) shows the time-dependent evolution of hydrogen during the photolysis under UV irradiation. It can be seen that hydrogen production increased with irradiation time for both PET and PLA. In all cases, higher yields were observed in the water than in NaOH suspensions, indicating that water conditions favour hydrogen evolution.

The photolysis of PLA mostly demonstrated higher yields of all the gaseous products which can be explained by the simpler molecular

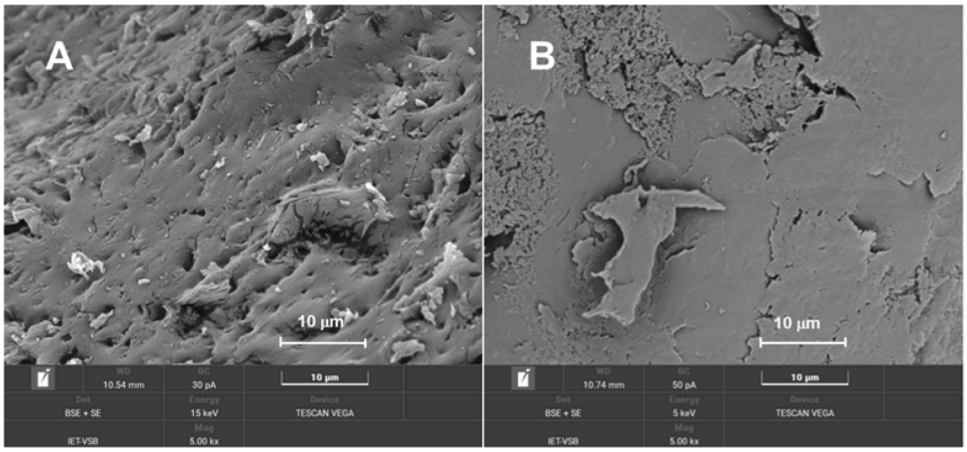

Fig. 3. SEM micrographs of PLA microplastics used for photolysis. (A) Original microplastics and (B) microplastics after 24 h in water.

Table 3
Real and theoretical compositions of studied microplastics.

Microplastics	O (wt%)	C (wt%)	H (wt%)
PET	31.03	63.77	5.20
PET (theor.)	33.33	62.50	4.17
PLA	44.14	49.97	5.88
PLA (theor.)	44.44	50.00	5.56

Note: The PET monomer formula is $C_{10}H_8O_4$ and the PLA monomer formula is $C_3H_4O_2$

structure of PLA facilitating the cleavage of ester bonds. PET contains aromatic rings which can lead to the formation of more stable degradation products in the liquid phase (terephthalic acid) which is further discussed. The hydrogen yields obtained in the water and NaOH suspensions for 4 h are shown in Fig. 1. A decrease in the hydrogen and methane yields in the NaOH suspensions was observed for both plastics. However, in the case of PLA, carbon monoxide production increased under alkaline conditions. Despite this, the total yield of gaseous products (H_2+CH_4+CO) decreased compared to that under water conditions.

3.2.1. Analysis of microplastics by SEM

Microplastic degradation was investigated using electron scanning microscopy, as shown in Figs. 2 and 3. In the SEM micrographs, the PET and PLA particles after irradiation for 24 h are compared with the original particles without any treatment. The surface of the PET microplastics became smooth after photolysis in water and even smoother after photolysis in the NaOH suspension. A similar observation was made for PLA microplastics after photolysis in water. During photolysis in the NaOH suspension, the PLA particles were completely dissolved.

3.2.2. Analysis of microplastics by FTIR

3.2.2.1. Analysis of PET microplastics. Structural changes in both microplastic materials due to photolysis in the water and NaOH suspensions were investigated by FTIR. The FTIR spectra of the PET are shown in Fig. 4. One spectrum of untreated PET microplastics labelled simply as "PET" was used for comparison. Two spectra of the PET microplastics treated in water and the NaOH solution under UV irradiation are labelled as "PET+H_2O+UV" and "PET+NaOH+UV", respectively.

In the spectrum of "PET", two weak bands at 2967 and 2890 cm^{-1} correspond to the asymmetric and symmetric stretching vibrations of C-H in CH_2 groups. The strong band at 1726 cm^{-1} can be assigned to the stretching vibrations of C=O. The bands at 1267 and 1098 cm^{-1} can be attributed to the (C=O)–O and O-CH_2 stretching vibrations, respectively. A medium band at 727 cm^{-1} can be assigned to the ring C–C bending and ring C–H out of plane vibrations [48,49] or the bending vibration of HO-C=O in COOH groups [50].

The spectrum of PET after photolysis in NaOH (PET + NaOH +UV) was identical to that of the untreated PET. The spectrum after photolysis in water (PET+H_2O+UV) shows weak bands at 2997 and 2945 cm^{-1}, corresponding to the asymmetric and symmetric stretching C-H

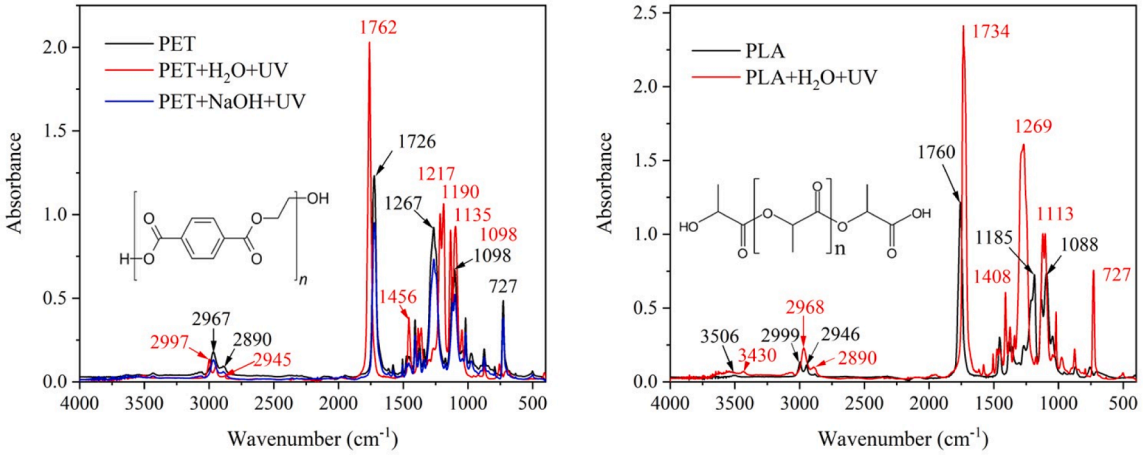

Fig. 4. FTIR spectra of the PET (left) and PLA (right) microplastics after photolysis for 24 h.

vibrations of the CH_2 groups. The strong bands at 1762 and 1217–1098 cm^{-1} correspond to C═O and C-O stretching vibrations, respectively [51,52]. The weak band at 1456 cm^{-1} could be assigned to the deformation vibration of the O-H group [51,52].

For the photolysis of PET, the Norrish II and I mechanisms have been referred to in the literature. The intramolecular Norrish II process leads to the formation of benzoic acid and CH_2=C< ended aliphatic compounds [53,54]. The Norrish process I was found to produce CO, CO_2, benzoic acid, benzaldehyde, formate, and aliphatic alcohols *via* hydrogen abstraction and recombination of various radicals [53]. Day and Willes [54] identified that more than 90 % of CO_2, CO, and other compounds were hydrogen, methane, water, ethylene, methanol, butane, acetic acid, formaldehyde, benzene, and toluene. Fechine et al. [55] recognized the Norrish I mechanism leading to the formation of mono or dihydroxy terephthalate and aromatic carboxyl acid end-groups. Chamas et al. [56] reported that PET hydrolysis forms terephthalic acid and ethylene glycol. In general, the degradation processes of plastics depend on external conditions, such as temperature, the presence of oxygen, and the intensity and energy of irradiation.

In this study, the degradation products were analysed by HPLC/HRTMS in full scan mode, and the chromatograms were carefully investigated for the presence of DPs. Only one degradation product was identified. This product was formed in the suspension after the photocatalysis of PET in the NaOH suspension. An *m/z* of 165.0139 was observed, suggesting the presence of terephthalic acid, whose predicted *m/z* of [M-H]- was 165.0193. In addition, the fragment observed at an *m/z* of 121.0227 (and theoretical *m/z* of 121.0295) indicated the presence of benzoic acid which proved that the detected compound was terephthalic acid. The concentration of terephthalic acid was 2.25 mg L^{-1}. For comparison, the limit of detection (LOD) for terephthalic acid was 1.00 mg L^{-1}. Fig. 8S shows the HPLC/HRTMS analysis of PET after photocatalysis.

3.2.2.2. Analysis of PLA microplastics. The spectra of PLA microplastics are shown in Fig. 4. In analogy with the previous spectra of PET, one can see the spectra of untreated PLA and treated PLA microplastics. The spectrum of untreated PLA microplastics ("PLA") shows broad bands corresponding to O-H groups at approximately 3500 cm^{-1}. Bands of the stretching C-H vibrations of the-CH_3 and -CH groups were observed at 2999 and 2946 cm^{-1}, respectively. Other bands at 1760, 1185, and 1088 cm^{-1} can be assigned to carbonyl vibrations, such as C═O, C-O, and C–O–C ones, respectively [57].

In the FTIR spectrum of the PLA microplastics after photolysis in water, a small band at 3430 cm^{-1} was observed, which can be explained by -OH stretching vibrations. The weak bands at 2968 and 2890 cm^{-1} can be assigned to the stretching C-H vibrations of the-CH_3 and -CH groups of lactic acid [50]. The strong bands at 1734 and 1269 cm^{-1} can be attributed to the stretching of C═O and C-O vibrations, respectively [50,58,59]. A band at 1113 cm^{-1} can be explained by the deformation vibrations of C-H [58,59] and a band at 727 cm^{-1} by the bending vibration of HO-C═O in COOH groups [50]. The FTIR spectrum of the PLA microplastics in the NaOH suspension is not shown in Fig. 4 because the microplastics were completely dissolved.

The formation of lactic acid after photolysis can, in principle, be caused by i) hydrolysis [56,60,61] and ii) the Norrish II mechanism [57,62]. Unlike bare hydrolysis, which is slow and requires a much longer time than 24 h to produce a remarkable amount of lactic acid, the Norrish mechanism II is realistic. The photolysis of PLA, leading to the formation of lactic acid, was also proposed by Deal et al. [63] using ^{13}C tagged lactic acid. The degradation products in the PLA suspensions were also analysed by LC/HRTMS; however, no compounds were identified. The LOD of lactic acid was 12.5 mg L^{-1}; therefore, lactic acid could be in suspensions at concentrations below the LOD.

3.3. Photocatalytic degradation of microplastics

Photocatalysis in this study was used to facilitate light-driven reactions on the surfaces of used photocatalysts, such as TiO_2 and g-C_3N_4, which absorb light energy and generate electron-hole pairs. The photogenerated electrons can reduce hydrogen ions (from water or degradation products) to molecular hydrogen, whereas holes can oxidise organic fragments. The efficiency of this process depends on the properties, stability, and reaction conditions of the photocatalyst used.

The photocatalytic degradation of PET and PLA microplastics was performed in the presence of photocatalysts, such as titanium dioxide and graphitic carbon nitride. These experiments were also performed under UV irradiation at 254 nm because UV irradiation has higher photon energy compared to visible irradiation (possible for g-C_3N_4), which allows us to accelerate the degradation reactions and obtain measurable results within shorter experimental times. In addition, the results obtained can be directly compared with those obtained by photolysis performed under the same UV irradiation.

Titanium dioxide (Degussa P25) was obtained as a commercial product. Graphitic carbon nitride was synthesised from melamine in the laboratory and subsequently exfoliated at 500 °C for 3 h. The thermal exfoliation of g-C_3N_4 was found to be a simple procedure for the synthesis of highly efficient photocatalyst [44–46]. Some characteristics of both photocatalysts are shown in the Supplementary Materials.

As shown in Fig. 5, more gaseous products, such as hydrogen, methane, and carbon monoxide, were formed in comparison to photolysis. Similar to photolysis, the product yields from PLA were higher than those from PET. The decrease in the product yield in the NaOH suspensions was also remarkable. A detailed analysis was performed for hydrogen which was the dominant gaseous product.

Fig. 6 shows the hydrogen yields over time for the photocatalytic degradation of microplastics using both photocatalysts. The increased hydrogen yields were similar to those obtained by photolysis. The yields of hydrogen evolved in the water suspensions were higher than those obtained in the NaOH suspensions, which is in line with photolysis.

3.4. Mechanisms of hydrogen evolution

3.4.1. Hydrogen evolution by photolysis

As shown in Fig. 1, hydrogen, methane, and carbon monoxide were formed during photolysis, but hydrogen was the dominant gaseous product. The hydrogen yields after 4 h of irradiation are summarised in Table 4. In general, the presence of NaOH in the suspensions led to a significant decrease in hydrogen evolution compared with in that water-based systems, especially for PET. However, in the case of PLA, the addition of TiO_2 to the NaOH suspension slightly increased the hydrogen yield compared to photolysis, indicating the partial photocatalytic activity of TiO_2, even under alkaline conditions. Nevertheless, the hydrogen yield was lower than that of the water suspension with TiO_2.

The mean decrease of the hydrogen yields in time was 2.0 and 1.3 for PET and PLA, respectively, see Fig. 9S. This is in line with the neutralisation of two carboxylic groups in terephthalic acid and one carboxylic group in lactic acid. (It should be noted that the theoretical pH of the 0.2 mol L^{-1} NaOH solution is 13.3).

The evolution of hydrogen under the photolysis can be described by the reaction of two hydrogen radicals [64]

$$H^{\bullet} + H^{\bullet} \rightarrow H_2 \quad (4)$$

Based on the decrease of hydrogen yields in the NaOH suspensions mentioned above one can assume the photoreaction of carboxyl groups to form hydrogen radicals [65]

$$R\text{-}COOH \rightarrow R\text{-}COO^{\bullet} + H^{\bullet} \quad (5)$$

The formation of carbon monoxide and methane can be explained by the reduction of carbon dioxide resulted from the photoreaction of

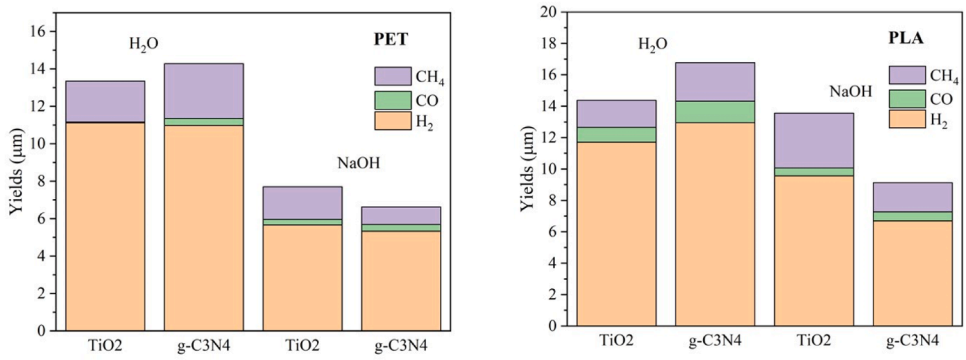

Fig. 5. Yields of the three main gaseous products of PET and PLA degradation after 4 h (left) and hydrogen yields during photocatalysis (right) under irradiation at 254 nm.

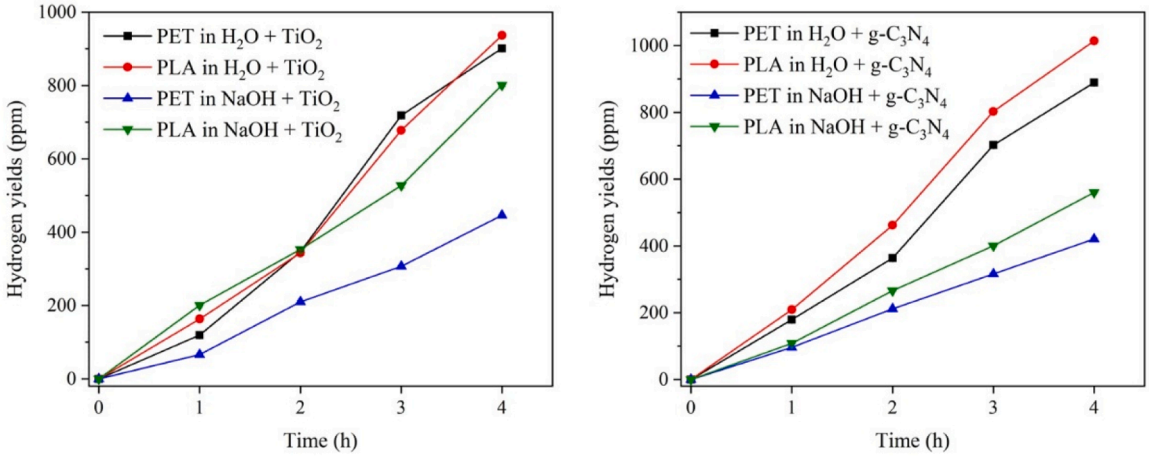

Fig. 6. Hydrogen yields during photocatalysis of microplastics suspended in water and NaOH solutions with TiO_2 (left) and g-C_3N_4 (right) photocatalysts under irradiation at 254 nm.

Table 4
Comparison of hydrogen yields after 4 h of UV irradiation (254 nm).

MPs	Hydrogen yields (ppm)					
	water	water TiO_2	water g-C_3N_4	NaOH	NaOH TiO_2	NaOH g-C_3N_4
PLA	800	937	1014	663	801	560
PET	827	901	889	454	446	420

carboxyl groups [65] as follows

$$\text{R-COOH} \rightarrow \text{R-H} + CO_2 \quad (6)$$

$$CO_2 + H_2 \rightarrow CO + H_2O\ (l) \quad (7)$$

$$CO_2 + 4\ H_2 \rightarrow CH_4 + 2\ H_2O\ (l) \quad (8)$$

The reactions (7) and (8) take place in water and calculated standard reaction enthalpies and Gibb's energies are $\Delta_r H^0_{298}$ = -2.84 kJ mol^{-1} and $\Delta_r G^0_{298}$ = 20.1 kJ mol^{-1} for the reaction (7) and $\Delta_r H^0_{298}$ = -253 kJ mol^{-1} and $\Delta_r G^0_{298}$ = -130 kJ mol^{-1} for the reaction (8). The input data are listed in Table 3S. The reaction (7) is not spontaneous, but the necessary energy was supplied by UV irradiation. For example, the formation of methane by the cracking bonds of -CH_3 groups cannot occur for terephthalic acid. However, this possibility cannot be excluded in the case of lactic acid.

Based on the stoichiometry of the reactions (7) and (8), it is clear that the reaction (5) does not provide a sufficient amount of hydrogen radicals from the PET and PLA microplastics for the reaction (4). Other reactions that provided hydrogen radicals for the formation of hydrogen must proceed. For example, the formation of hydrogen radicals from the photoreaction products could be explained by the breaking of C-H and /or O-H groups [66,67]. In the NaOH suspensions, R-COOH is neutralised into R-COO^-, and the reaction (5) cannot occur. Moreover, in these alkaline suspensions, the hydrogen radicals can react with hydroxide ions [64] which also explains the decrease of hydrogen yields as follows

$$H^\bullet + OH^- \rightarrow H_2O + e^- \quad (9)$$

3.4.2. *Hydrogen evolution by photocatalysis*

In general, any photocatalytic process in a liquid phase consists of several steps, such as the adsorption of reactants from a liquid on a photocatalyst, reaction on its surface, and desorption of reaction products back to the liquid. In the case of microplastic suspensions, the contact between microplastic particles (reactants) and photocatalysts is limited. A more realistic process consists of i) the photolysis of microplastics forming hydrogen and some degradation products and ii) the photocatalytic evolution of another hydrogen from the degradation products which release hydrogen ions at the photocatalyst surfaces. It is commonly accepted, e.g. [68], that the catalytic hydrogen evolution mechanism consists of several steps under acidic conditions

$$H_3O^+ + e^- + X \rightarrow X\text{-}H + H_2O\ \text{(Volmer)} \quad (10)$$

$$X\text{-}H + H_3O^+ + e^- \rightarrow H_2 + H_2O + X\ \text{(Heyrovský)} \quad (11)$$

$$2\ X\text{-}H \rightarrow 2\ X + H_2 \text{ (Tafel)} \quad (12)$$

and under alkaline conditions

$$H_2O + e^- + X \rightarrow X\text{-}H + OH^- \text{ (Volmer)} \quad (13)$$

$$H_2O + e^- + X\text{-}H \rightarrow X + H_2 + OH^- \text{ (Heyrovský)} \quad (14)$$

where X refers to an active site on the catalyst, and X-H indicates an adsorbed hydrogen atom on the catalyst. The photocatalytic process with PET and PLA was performed in an inert helium atmosphere; therefore, no reactive oxygen species (ROS) were generated in the photocatalytic reactions. Under these conditions, the photocatalysts provide only photoinduced electrons and holes. The overall hydrogen yields are summarised in Table 4 and Fig. 5.

Fig. 5 also shows the total yields of all gaseous products. This decrease was significant for the NaOH suspensions. When g-C_3N_4 was used in water suspensions, the yields were higher than those of TiO_2. However, in the NaOH suspensions, the opposite yields were obtained. This can be attributed to the lower stability of g-C_3N_4 under alkaline conditions which was studied further. The TiO_2 photocatalyst was stable during all experiments, even in the NaOH suspensions. This was confirmed by XRD; see the XRD patterns in Fig. 10S.

3.5. Stability of g-C_3N_4 in NaOH suspensions

3.5.1. Analysis by XPS

The lower stability of g-C_3N_4 was verified by the XPS analysis of g-C_3N_4 treated in the water and NaOH suspensions under UV irradiation for 4 h. The XPS elemental analysis results are summarised in Table 5. The changes in the nitrogen content and C/N fractions indicate the release of nitrogen from the g-C_3N_4 structure due to the presence of NaOH.

The typical nitrogen spectra of g-C_3N_4 are shown in Fig. 7. These were fitted by four peaks with positions at approximately 398.8, 400.0, 401.4 and 404.2 eV. Two peaks at 398.8 and 400.0 eV can be attributed to the sp^2 hybridized nitrogen (C═N-C) and nitrogen of tertiary amine (N-(C)3), respectively. The peak at 401.4 eV can be ascribed to the C-N-H bond. The peak at 404.2 eV can be explained by the π–π* (HOMO–LUMO) transition. To see some changes in the N atoms in the g-C_3N_4 structure, the intensities corresponding to (N-(C)3) and C-N-H bonds were related to those of C═N-C bonds, creating relatively stable aromatic rings (Table 6).

The fractions of intensities related to the N-(C)3 and C═N-C bonds indicate the loss of nitrogen atoms connecting the heptazine units. The HOMO levels of the melem monomer are formed from nitrogen p_z orbitals, and the LUMO levels consist of the p_z orbital of carbon [69]. The loss of nitrogen atoms indicates the loss of electrons which can be photoexcited over the g-C_3N_4 band gap and, in turn, can be utilised for the reduction of hydrogen ions to form hydrogen according to the reactions (10)-(14). It also explains the reduced hydrogen yield in the NaOH suspensions (Table 4).

In the water suspensions, the hydrogen ions involved in the reactions (10)-(12) were reduced by photoinduced electrons by the photocatalysts. Hydrogen ions are produced by the dissociation of the degradation products (organic acids) released by photolysis. When NaOH was present, the hydrogen ions were neutralised by hydroxide ions, and the evolution of hydrogen was possible only from water molecules, according to the reactions (13) and (14).

The XPS carbon spectra of g-C_3N_4 are shown in Fig. 8. The C 1 s spectra were fitted by two peaks with positions at about 288.5 and 288.4 eV and 286.2 and 285.5 eV. The peaks at 288.4 and 288.5 eV can be ascribed to sp2hybridized carbon (N-C═N). The other peaks at 286.2 or 285.5 eV can be attributed to C-C (284.8 eV), C-O (286–287 eV), and C-N (286 eV). The latter peak is more intense in g-C_3N_4 treated with NaOH which implies that more C-O bonds are formed by the reactions of air oxygen with the nitrogen defects when g-C_3N_4 comes into contact with air. The similar effect was already observed when g-C_3N_4 was thermally synthesised in the nitrogen and argon atmospheres [44,70]. The higher oxygen content in g-C_3N_4 after treatment with NaOH (Tab. (5)) can be explained by the presence of residual NaOH, as shown in Fig. 11S. The XPS spectra of O 1 s are shown in Fig. 9.

In the case of g-C_3N_4 treated in water, the main peak centred at 533.1 eV corresponds to slight surface oxidation, and a small peak centred at 534.8 eV can be ascribed to adsorbed water. In contrast, treatment with NaOH resulted in a significantly higher amount of oxygen on the surface of g-C_3N_4. The spectrum contains a contribution ascribed to a slightly oxidised surface shifted to 533.9 eV with approximately the same intensity as that of g-C_3N_4 treated in water. The second and more intense peak centred at 532.0 eV can be ascribed to the -OH groups [71] which can be attributed to OH^- ions from the residual NaOH.

3.5.2. Analysis by XRD

The structure of g-C_3N_4 treated in the water and NaOH suspensions was analysed by XRD, as shown in Fig. 10. Two XRD patterns typical of graphitic carbon nitride were observed (JCPDS 87–1526). The more intense diffraction (002) at approximately 27.7° 2θ corresponds to the interlayer stacking of heptazine planes, and the less intense diffraction (100) at approximately 13.1° 2θ corresponds to the in-plane arrangement of the heptazine units linked by nitrogen. Remarkably, the (100) peak of g-C_3N_4 treated in the NaOH suspension is broader than that treated in water. The peak broadening can be explained by the disruption of the in-plane ordering of the nitrogen-linked heptazine units owing to the loss of connecting nitrogen atoms.

3.5.3. Analysis by FTIR

The changes in the structure of g-C_3N_4 treated in the water and NaOH suspensions were also studied by FTIR, as shown in Fig. 11. The most important differences are visible in the range of N–H stretching vibrations corresponding to 3248, 3171, and 3091 cm^{-1}.

Another remarkable decrease in absorbance was observed between 1634 and 1240 cm^{-1} which is associated with C═N and C-N stretching vibrations [72,73]. The typical bands around 808 cm^{-1}, which are associated with the breathing mode of the triazine units, remained unchanged. These findings indicate the partial destruction of heptazine units and their connections.

Some reaction products are likely to be formed by the decomposition of g-C_3N_4 and can be expected in both the gas and liquid phases. However, given the current detection limits of the analytical methods used, these were not detected.

Table 5
XPS analysis of g-C_3N_4 after 4 h of irradiation at 254 nm.

g-C_3N_4	C (at%)	O (at%)	N (at%)	Na (at%)	C/N
UV + H_2O	44.04	4.55	51.41		0.857
UV + NaOH	46.15	7.63	41.82	4.40	1.104

4. Conclusion

This study demonstrates the potential of PET and PLA microplastics as hydrogen sources through photoreforming under UV irradiation. Thermodynamic calculations indicated that hydrogen evolution from these plastics is feasible, with a lower Gibbs free energy than that of water splitting.

Photolysis experiments confirmed that hydrogen was the main product, although methane and carbon monoxide were also produced. The introduction of NaOH reduced the hydrogen yield owing to the neutralisation of carboxylic groups and the scavenging of hydrogen radicals with hydroxide ions. The addition of TiO_2 and g-C_3N_4 photocatalysts (i.e. photocatalytic experiments) enhanced hydrogen evolution, with g-C_3N_4 outperforming TiO_2 in the water suspensions. However, its structural stability was compromised under alkaline

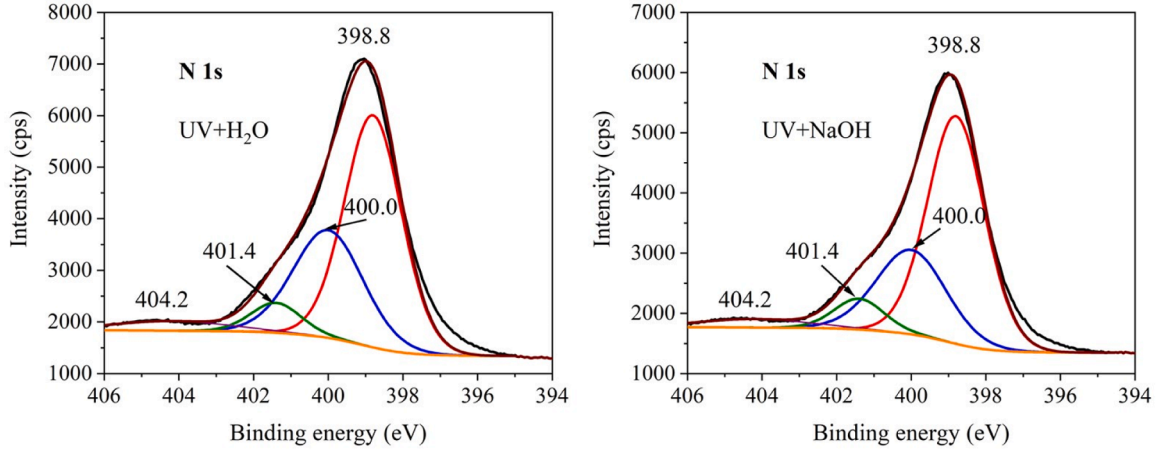

Fig. 7. XPS spectra of N 1 s of g-C_3N_4 after UV irradiation for 4 h in water (left) and NaOH suspensions (right).

Table 6
XPS relative intensities of specific N bonds in g-C_3N_4.

g-C_3N_4	C═N-C	N-(C)3	C-N-H	N-(C)3/C═N-C	C-N-H/C═N-C
UV + H_2O	56.63	32.09	6.39	0.567	0.113
UV + NaOH	60.87	27.57	7.16	0.453	0.118

conditions leading to decreased photocatalytic efficiency. The combination of surface (SEM, XPS), structural (XRD, FTIR), and compositional (EA and LC-HRTMS) analyses allowed us to comprehensively interpret the degradation behaviour of both microplastics and photocatalysts, linking the observed gas evolution patterns to specific structural changes.

This work shows the mechanism of microplastic degradation and

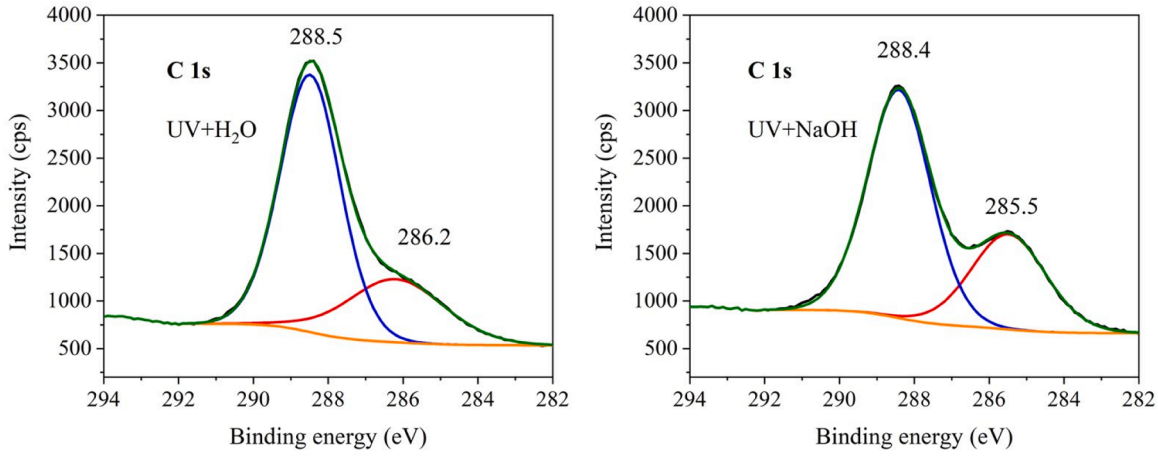

Fig. 8. XPS spectra of C 1 s of g-C_3N_4 after UV irradiation for 4 h in water (left) and NaOH suspensions (right).

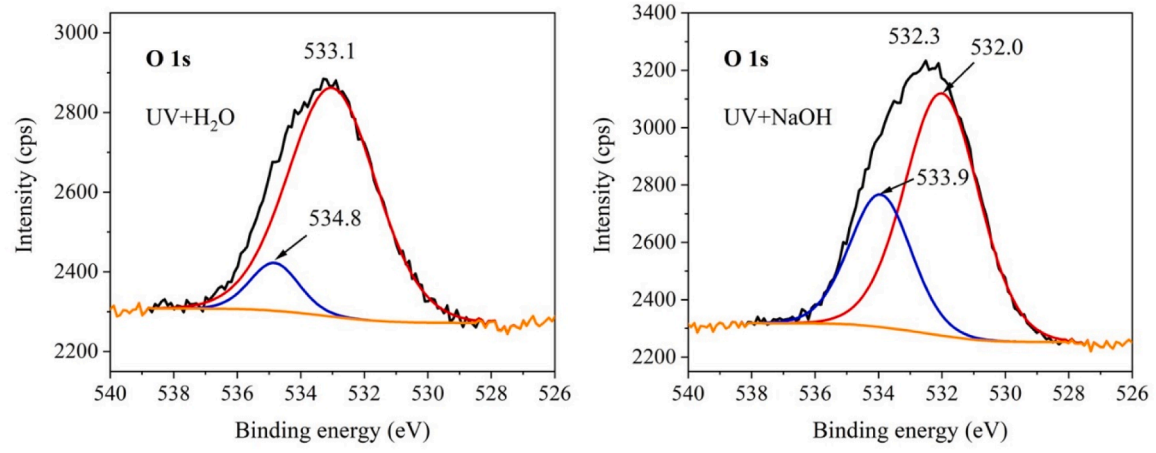

Fig. 9. XPS spectra of O 1 s of g-C_3N_4 after UV irradiation for 4 h in water (left) and NaOH suspensions (right).

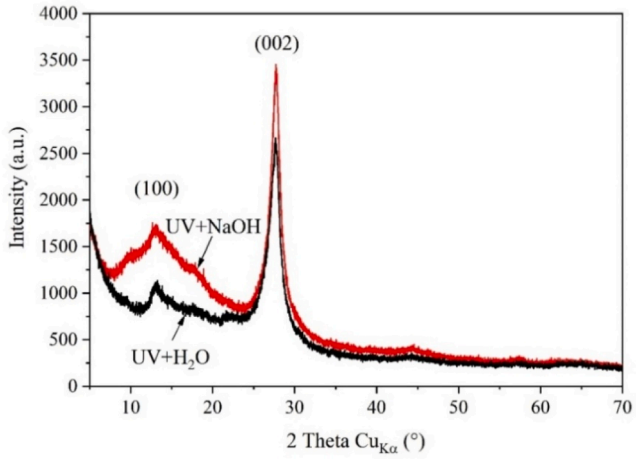

Fig. 10. XRD patterns of g-C_3N_4 after UV irradiation for 4 h in water and NaOH suspensions.

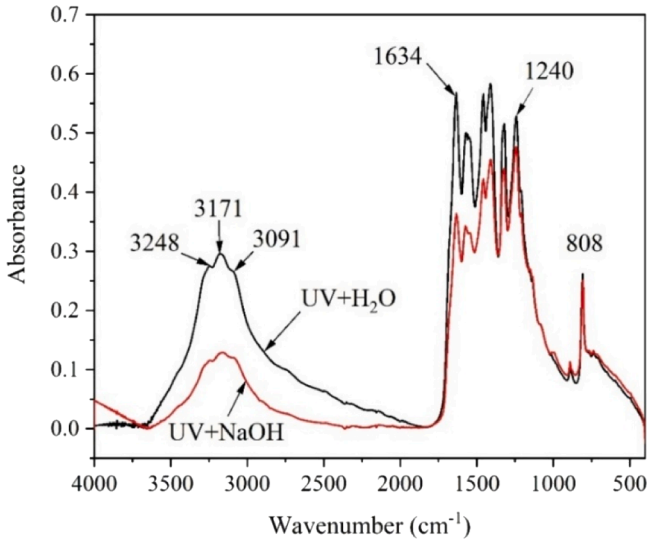

Fig. 11. FTIR spectra of g-C_3N_4 after UV irradiation for 4 h in water and NaOH suspensions.

hydrogen evolution, and indicates that photoreforming could serve as both a plastic waste treatment strategy and a renewable hydrogen production method. Our future research will focus on optimising the reaction conditions, improving the photocatalyst stability, and developing separation techniques to enhance the hydrogen purity.

CRediT authorship contribution statement

Řeháčková Lenka: Methodology, Investigation, Formal analysis. **Praus Petr:** Writing – original draft, Supervision, Methodology, Investigation, Formal analysis, Data curation, Conceptualization. **Gavlová Anna:** Investigation, Data curation. **Filip-Edelmanová Miroslava:** Investigation, Data curation. **Kočí Kamila:** Writing – original draft, Methodology, Investigation, Data curation, Conceptualization. **Bednář Petr:** Investigation, Data curation. **Bednárek Jan:** Investigation, Data curation. **Škuta Radim:** Investigation, Data curation. **Koštejn Martin:** Investigation, Data curation.

Declaration of Competing Interest

The authors declare that they have no known competing financial interests or personal relationships that could have appeared to influence the work reported in this paper.

Acknowledgements

This study was financially supported by the European Union under the REFRESH – Research Excellence For REgion Sustainability and High-tech Industries (Project No. CZ.10.03.01/ 00/22_003/0000048) via the Operational Programme Just Transition and by the OP JAK project "INOVO!!!" (No. CZ.02.01.01/00/23_021/0008588) provided by the Ministry of Education, Youth, and Sports and co-financed by the European Union. The authors also thank the Large Research Infrastructure ENREGAT (Project No. LM2023056) and VSB-Technical University of Ostrava (Project No. SP 2024/009).

Appendix A. Supporting information

Supplementary data associated with this article can be found in the online version at doi:10.1016/j.jece.2025.116998.

Data Availability

Data will be made available on request.

References

[1] F. Zhang, Y. Zhao, D. Wang, M. Yan, J. Zhang, P. Zhang, T. Ding, L. Chen, C. Chen, Current technologies for plastic waste treatment: a review, J. Clean. Prod. 282 (2021) 124523.
[2] I.E. Napper, R.C. Thompson, Plastics and the environment, Annu. Rev. Environ. Resour. 48 (2023) 55–79.
[3] R.C. Thompson, Y. Olsen, R.P. Mitchell, A. Davis, S.J. Rowland, A.W.G. John, D. McGonigle, A.E. Russell, Lost at sea: where is all the plastic? Science 304 (2004) 838. -838.
[4] T.A. Kurniawan, A. Haider, H.M. Ahmad, A. Mohyuddin, H.M. Umer Aslam, S. Nadeem, M. Javed, M.H.D. Othman, H.H. Goh, K.W. Chew, Source, occurrence, distribution, fate, and implications of microplastic pollutants in freshwater on environment: A critical review and way forward, Chemosphere 325 (2023) 138367.
[5] S. Ghosh, J.K. Sinha, S. Ghosh, K. Vashisth, S. Han, R. Bhaskar, Microplastics as an emerging threat to the global environment and human health, Sustainability 15 (2023) 10821.
[6] Y. Zhao, J. Song, K. Cheng, Z. Liu, F. Yang, Migration and remediation of typical contaminants in soil and groundwater: a state of art review, Land Degrad. Dev. 35 (2024) 2700–2715.
[7] E. Winiarska, M. Jutel, M. Zemelka-Wiacek, The potential impact of nano- and microplastics on human health: Understanding human health risks, Environ. Res. 251 (2024) 118535.
[8] J. Oza, V. Rabari, V.K. Yadav, D.K. Sahoo, A. Patel, J. Trivedi, A. Systematic, Review on microplastic contamination in fishes of asia: polymeric risk assessment and future prospectives, Environ. Toxicol. Chem. 43 (2024) 671–685.
[9] L. Jia, L. Liu, Y. Zhang, W. Fu, X. Liu, Q. Wang, M. Tanveer, L. Huang, Microplastic stress in plants: effects on plant growth and their remediations, Front. Plant Sci. 14 (2023) 1226484.
[10] S. O'Brien, C. Rauert, F. Ribeiro, E.D. Okoffo, S.D. Burrows, J.W. O'Brien, X. Wang, S.L. Wright, K.V. Thomas, There's something in the air: a review of sources, prevalence and behaviour of microplastics in the atmosphere, Sci. Total Environ. 874 (2023) 162193.
[11] C. Vitali, R.J.B. Peters, H.-G. Janssen, M.W.F. Nielen, Microplastics and nanoplastics in food, water, and beverages; part I. occurrence, TrAC Trends Anal. Chem. 159 (2023) 116670.
[12] R.C. Hale, M.E. Seeley, M.J. La Guardia, L. Mai, E.Y. Zeng, A global perspective on microplastics, JGR Oceans 125 (2020) e2018JC014719.
[13] G. Suzuki, N. Uchida, K. Tanaka, O. Higashi, Y. Takahashi, H. Kuramochi, N. Yamaguchi, M. Osako, Global discharge of microplastics from mechanical recycling of plastic waste, Environ. Pollut. 348 (2024) 123855.
[14] A.I. Osman, M. Hosny, A.S. Eltaweil, S. Omar, A.M. Elgarahy, M. Farghali, P.-S. Yap, Y.-S. Wu, S. Nagandran, K. Batumalaie, S.C.B. Gopinath, O.D. John, M. Sekar, T. Saikia, P. Karunanithi, M.H.M. Hatta, K.A. Akinyede, Microplastic sources, formation, toxicity and remediation: a review, Environ. Chem. Lett. 21 (2023) 2129–2169.
[15] M.G. Kibria, N.I. Masuk, R. Safayet, H.Q. Nguyen, M. Mourshed, Plastic waste: challenges and opportunities to mitigate pollution and effective management, Int. J. Environ. Res. 17 (2023) 20.
[16] A. Gavlová, P. Jachimowicz, P. Praus, P. Bednář, Environment changes everything. How relevant are laboratory studies of sorption of pollutants on microplastics? a critical review, J. Environ. Chem. Eng. 13 (2025) 115655.

[17] S. Ye, M. Cheng, G. Zeng, X. Tan, H. Wu, J. Liang, M. Shen, B. Song, J. Liu, H. Yang, Y. Zhang, Insights into catalytic removal and separation of attached metals from natural-aged microplastics by magnetic biochar activating oxidation process, Water Res. 179 (2020) 115876.

[18] J. Chen, J. Wu, P.C. Sherrell, J. Chen, H. Wang, W.-x Zhang, J. Yang, How to build a microplastics-free environment: strategies for microplastics degradation and plastics recycling, advances, Science 9 (2022) 2103764.

[19] Y. Gao, Y. Liu, Removal of microplastics by coagulation treatment in waters and prospect of recycling of separated microplastics: a mini-review, J. Environ. Chem. Eng. 10 (2022) 108197.

[20] M. Zandieh, E. Griffiths, A. Waldie, S. Li, J. Honek, F. Rezanezhad, P. Van Cappellen, J. Liu, Catalytic and biocatalytic degradation of microplastics, Exploration 4 (2024) 20230018.

[21] U. Anand, S. Dey, E. Bontempi, S. Ducoli, A.D. Vethaak, A. Dey, S. Federici, Biotechnological methods to remove microplastics: a review, Environ. Chem. Lett. 21 (2023) 1787–1810.

[22] M. Carnevale Miino, S. Galafassi, R. Zullo, V. Torretta, E.C. Rada, Microplastics removal in wastewater treatment plants: a review of the different approaches to limit their release in the environment, Sci. Total Environ. 930 (2024) 172675.

[23] Y. Guo, X. Xia, J. Ruan, Y. Wang, J. Zhang, G.A. LeBlanc, L. An, Ignored microplastic sources from plastic bottle recycling, Sci. Total Environ. 838 (2022) 156038.

[24] W. Nabgan, B. Nabgan, T.A. Tuan Abdullah, M. Ikram, A.H. Jadhav, M.W. Ali, A. A. Jalil, Hydrogen and value-added liquid fuel generation from pyrolysis-catalytic steam reforming conditions of microplastics waste dissolved in phenol over bifunctional Ni-Pt supported on Ti-Al nanocatalysts, Catal. Today 400-401 (2022) 35–48.

[25] F. Ma, S. Wang, X. Gong, X. Liu, Z. Wang, P. Wang, Y. Liu, H. Cheng, Y. Dai, Z. Zheng, B. Huang, Highly efficient electrocatalytic hydrogen evolution coupled with upcycling of microplastics in seawater enabled via Ni3N/W5N4 janus nanostructures, Applied Catalysis B, Environ. Energy 307 (2022) 121198.

[26] X. Zhang, M. Jun, W. Zu, M. Kim, K. Lee, L.Y.S. Lee, Photoreforming of microplastics: challenges and opportunities for sustainable environmental remediation, Small 20 (2024) 2403347.

[27] Y. Jiang, H. Zhang, L. Hong, J. Shao, B. Zhang, J. Yu, S. Chu, An integrated plasma–photocatalytic system for upcycling of polyolefin plastics, ChemSusChem 16 (2023) e202300106.

[28] G. Reimonn, T. Lu, N. Gandhi, W.-T. Chen, Review of Microplastic Pollution in the Environment and Emerging Recycling Solutions, J. Renew. Mater. 7 (2019) 1251–1268.

[29] C.Y. Toe, C. Tsounis, J. Zhang, H. Masood, D. Gunawan, J. Scott, R. Amal, Advancing photoreforming of organics: highlights on photocatalyst and system designs for selective oxidation reactions, Energy Environ. Sci. 14 (2021) 1140–1175.

[30] A. Samal, C. Mohanty, N. Das, R. Das, M.F. Kühnel, A review on metal phosphate based graphene hybrids: emerging composite materials for vast applications, Mater. Today Chem. 38 (2024) 102096.

[31] B. Xia, Y. Zhang, B. Shi, J. Ran, K. Davey, S.-Z. Qiao, Photocatalysts for hydrogen evolution coupled with production of value-added chemicals, small, Methods 4 (2020) 2000063.

[32] M. Du, Y. Zhang, S. Kang, X. Guo, Y. Ma, M. Xing, Y. Zhu, Y. Chai, B. Qiu, Trash to treasure: photoreforming of plastic waste into commodity chemicals and hydrogen over MoS_2 Tipped CdS nanorods, ACS, Catalysis 12 (2022) 12823–12832.

[33] S. Zhang, H. Li, L. Wang, J. Liu, G. Liang, K. Davey, J. Ran, S.-Z. Qiao, Boosted photoreforming of plastic waste via defect-rich $NiPS_3$ nanosheets, J. Am. Chem. Soc. 145 (2023) 6410–6419.

[34] Z. Ma, S. Zhan, Y. Zhang, A. Kuklin, Y. Chen, Y. Lin, H. Zhang, X. Ren, H. Ågren, Y. Zhang, An electron transfer mediated mechanism for efficient photoreforming of waste plastics using a Ni_3S_4/ZnCdS heterojunction, adavanced, Materials 37 (2025) 2416581.

[35] T.T. Nguyen, K. Edalati, Impact of high-pressure columbite phase of titanium dioxide (TiO_2) on catalytic photoconversion of plastic waste and simultaneous hydrogen (H_2) production, J. Alloy. Compd. 1008 (2024) 176722.

[36] Z. Ya, L. Tang, D. Xu, H. Wang, S. Zhang, Photoreforming of waste plastic by B-doped carbon nitride nanotube: Atomic-level modulation and mechanism insights, AiChE J. (2025) e18740.

[37] C. Mohanty, A. Samal, N. Das, Concurrent photoreforming of polyethylene into commercial chemicals and hydrogen generation utilizing g-C_3N_4/Co_3O_4 Z-scheme heterostructure: a waste-to-wealth concept, Int. J. Hydrog. Energy 61 (2024) 84–93.

[38] P. Praus, Photoreforming for microplastics recycling: a critical review, J. Environ. Chem. Eng. 12 (2024) 112525.

[39] S.P. Shelake, D.N. Sutar, B.M. Abraham, T. Banerjee, A.V.S. Sainath, U. Pal, Emerging photoreforming process to hydrogen production: a future energy, Adv. Funct. Mater. 34 (2024) 2403795.

[40] A. Samal, N. Das, Shining Light on the Future: Photoreforming (PR) as a Solution to Plastic Trash: A Brief Review, Plastic Degradation and Conversion by Photocatalysis. From Waste to Wealth 2, American Chemical Society, 2024, pp. 223–248.

[41] A. Samal, N. Das, Mini-review on remediation of plastic pollution through photoreforming: progress, possibilities, and challenges, Environ. Sci. Pollut. Res. 30 (2023) 83138–83152.

[42] A. Chen, M.-Q. Yang, S. Wang, Q. Qian, Recent advancements in photocatalytic valorization of plastic waste to chemicals and fuels, Front. Nanotechnol. 3 (2021) 723120.

[43] S.H. Paiman, S.F. Md Noor, N. Ngadi, A.H. Nordin, N. Abdullah, Insight into photocatalysis technology as a promising approach to tackle microplastics pollution through degradation and upcycling, Chem. Eng. J. 467 (2023) 143534.

[44] P. Praus, A. Smýkalová, K. Foniok, V. Matějka, M. Kormunda, B. Smetana, D. Cvejn, The presence and effect of oxygen in graphitic carbon nitride synthetized in air and nitrogen atmosphere, Appl. Surf. Sci. 529 (2020) 147086.

[45] A. Smýkalová, B. Sokolová, K. Foniok, V. Matějka, P. Praus, Photocatalytic degradation of selected pharmaceuticals Using g-C_3N_4 and TiO_2, Nanomaterials, Nanomaterials 9 (2019) 1194.

[46] L. Svoboda, P. Praus, M.J. Lima, M.J. Sampaio, D. Matýsek, M. Ritz, R. Dvorský, J. L. Faria, C.G. Silva, Graphitic carbon nitride nanosheets as highly efficient photocatalysts for phenol degradation under high-power visible LED irradiation, Mater. Res. Bull. 100 (2018) 322–332.

[47] L. Mandelkern, R.G. Alamo, Thermodynamic Quantities Governing Melting, in: J. E. Mark (Ed.), Physical Properties of Polymers Handbook, Springer New York, New York, NY, 2007, pp. 165–186.

[48] M. Djebara, J.P. Stoquert, M. Abdesselam, D. Muller, A.C. Chami, FTIR analysis of polyethylene terephthalate irradiated by MeV He^+, Nucl. Instrum. Methods Phys. Res. Sect. B: Beam Interact. Mater. At. 274 (2012) 70–77.

[49] C. Ioakeimidis, K.N. Fotopoulou, H.K. Karapanagioti, M. Geraga, C. Zeri, E. Papathanassiou, F. Galgani, G. Papatheodorou, The degradation potential of PET bottles in the marine environment: An ATR-FTIR based approach, Sci. Rep. 6 (2016) 23501.

[50] C.D. Zeinalipour-Yazdi, C.R.A. Catlow, An experimental and computational IR and hybrid DFT-D3 study of the conformations of l-lactic and acrylic acid: new insight into the dehydration mechanism of lactic acid to acrylic acid, Phys. Chem. Chem. Phys. 21 (2019) 22331–22343.

[51] R.K. Soni, S. Soam, K. Dutt, Studies on biodegradability of copolymers of lactic acid, terephthalic acid and ethylene glycol, Polym. Degrad. Stab. 94 (2009) 432–437.

[52] N. Karthikeyan, J. Joseph Prince, S. Ramalingam, S. Periandy, Electronic [UV–Visible] and vibrational [FT-IR, FT-Raman] investigation and NMR–mass spectroscopic analysis of terephthalic acid using quantum Gaussian calculations, Spectrochim. Acta Part A: Mol. Biomol. Spectrosc. 139 (2015) 229–242.

[53] T. Grossetête, A. Rivaton, J.L. Gardette, C.E. Hoyle, M. Ziemer, D.R. Fagerburg, H. Clauberg, Photochemical degradation of poly(ethylene terephthalate)-modified copolymer, Polymer 41 (2000) 3541–3554.

[54] M. Day, D.M. Wiles, Photochemical degradation of poly(ethylene terephthalate). III. Determination of decomposition products and reaction mechanism, J. Appl. Polym. Sci. 16 (1972) 203–215.

[55] G.J.M. Fechine, M.S. Rabello, R.M. Souto Maior, L.H. Catalani, Surface characterization of photodegraded poly(ethylene terephthalate). The effect of ultraviolet absorbers, Polymer 45 (2004) 2303–2308.

[56] A. Chamas, H. Moon, J. Zheng, Y. Qiu, T. Tabassum, J.H. Jang, M. Abu-Omar, S. L. Scott, S. Suh, Degradation rates of plastics in the environment, ACS Sustain. Chem. Eng. 8 (2020) 3494–3511.

[57] T. Tosakul, P. Suetong, P. Chanthot, C. Pattamaprom, Degradation of polylactic acid and polylactic acid/natural rubber blown films in aquatic environment, J. Polym. Res. 29 (2022) 242.

[58] T. Ube, Y. Yoneyama, T. Ishiguro, In situ measurement of the pH-dependent transmission infrared spectra of aqueous lactic acid solutions, Anal. Sci. 33 (2017) 1395–1399.

[59] Y.-K. Chen, Y.-F. Lin, Z.-W. Peng, J.-L. Lin, Transmission FT-IR study on the adsorption and reactions of lactic acid and poly(lactic acid) on TiO_2, The, J. Phys. Chem. C. 114 (2010) 17720–17727.

[60] V. Verney, A. Ramoné, F. Delor-Jestin, S. Commereuc, M. Koutny, G. Perchet, J. Troquet, Melt viscoelastic assessment of poly(Lactic Acid) composting: influence of UV Ageing, Molecules 23 (2018) 2682.

[61] W. Limsukon, M. Rubino, M. Rabnawaz, L.-T. Lim, R. Auras, Hydrolytic degradation of poly(lactic acid): unraveling correlations between temperature and the three phase structures, Polym. Degrad. Stab. 217 (2023) 110537.

[62] Q. Li, J. Cao, J. Li, D. Li, B. Jing, J. Zhou, Z. Ao, Novel insights into photoaging mechanisms and environmental persistence risks of polylactic acid (PLA) microplastics: Direct and indirect photolysis, Sci. Total Environ. 954 (2024) 176350.

[63] A.M. Deal, B.N. Frandsen, V. Vaida, Lactic acid photochemistry following excitation of S0 to S1 at 220 to 250 nm, J. Phys. Org. Chem. 35 (2022) e4316.

[64] G.V. Buxton, C.L. Greenstock, W.P. Helman, A.B. Ross, Critical Review of rate constants for reactions of hydrated electrons, hydrogen atoms and hydroxyl radicals (·OH/·O− in Aqueous Solution, J. Phys. Chem. Ref. Data 17 (1988) 513–886.

[65] L.J. Mittal, J.P. Mittal, E. Hayon, Photo-induced decarboxylation of aliphatic acids and esters in solution. Dependence upon state of protonation of the carboxyl group, The, J. Phys. Chem. 77 (1973) 1482–1487.

[66] J. Jiang, H. Zhao, D. Xia, X. Li, B. Qu, Formation of free radicals by direct photolysis of halogenated phenols (HPs) and effects of DOM: a case study on monobromophenols, J. Hazard. Mater. 391 (2020) 122220.

[67] L. Qin, L. Yang, J. Yang, R. Weber, K. Ranguelova, X. Liu, B. Lin, C. Li, M. Zheng, G. Liu, Photoinduced formation of persistent free radicals, hydrogen radicals, and hydroxyl radicals from catechol on atmospheric particulate matter, iScience 24 (2021) 102193.

[68] F. Bao, E. Kemppainen, I. Dorbandt, R. Bors, F. Xi, R. Schlatmann, R. van de Krol, S. Calnan, Understanding the hydrogen evolution reaction kinetics of electrodeposited nickel-molybdenum in acidic, near-neutral, and alkaline conditions, ChemElectroChem 8 (2021) 195–208.

[69] X. Wang, K. Maeda, A. Thomas, K. Takanabe, G. Xin, J.M. Carlsson, K. Domen, M. Antonietti, A metal-free polymeric photocatalyst for hydrogen production from water under visible light, Nat. Mater. 8 (2009) 76–80.
[70] P. Praus, L. Řeháčková, J. Čížek, A. Smýkalová, M. Koštejn, J. Pavlovský, M. Filip Edelmannová, K. Kočí, Synthesis of vacant graphitic carbon nitride in argon atmosphere and its utilization for photocatalytic hydrogen generation, Sci. Rep. 12 (2022) 13622.
[71] J. Li, C. He, N. Xu, K. Wu, Z. Huang, X. Zhao, J. Nan, X. Xiao, Interfacial bonding of hydroxyl-modified g-C_3N_4 and $Bi_2O_2CO_3$ toward boosted CO_2 photoreduction: Insights into the key role of OH groups, Chem. Eng. J. 452 (2023) 139191.
[72] S.E. Rodil, A.C. Ferrari, J. Robertson, W.I. Milne, Raman and infrared modes of hydrogenated amorphous carbon nitride, J. Appl. Phys. 89 (2001) 5425–5430.
[73] S. Bhattacharyya, C. Cardinaud, G. Turban, Spectroscopic determination of the structure of amorphous nitrogenated carbon films, J. Appl. Phys. 83 (1998) 4491–4500.